

HIGH AVERAGE-POWER INDUCTION LINACS*

D. S. Prono, D. Barrett, E. Bowles,[†] G. J. Caporaso, Yu-Jiuan Chen,
J. C. Clark, F. Coffield, M. A. Newton, W. Nexsen, D. Ravenscroft, W. C. Turner,
and J. A. Watson

Lawrence Livermore National Laboratory
Livermore, CA 94550

Abstract

Induction linear accelerators (LIAs) are inherently capable of accelerating several thousand amperes of ~ 50 -ns duration pulses to > 100 MeV. In this paper we report progress and status in the areas of duty factor and stray power management. These technologies are vital if LIAs are to attain high average power operation.

Introduction

Induction linear accelerators (LIAs) are powered by causing a large, pulsed, time-varying current to once circle a ferrite annulus. This results in a large, time-varying, azimuthal magnetic field to be imbedded in the ferrite annulus. An electron beam threading the center of the annulus acts as the secondary of this pulsed transformer and is accelerated by the induced electromotive force. With proper electrical matching this low impedance 1:1 transformer arrangement allows for incremental acceleration of large electron beam currents. Stacking many such transformers in series and having the electron beam be the secondary common to all modules enables high beam voltages to be attained.

The physics design of the LIA generally addresses the issues of stable beam transport and emittance preservation; the constraints imposed by these issues can be summarized as follows. The exponential growth of the beam breakup (BBU) instability has a dependence

$$\text{BBU exponential growth} \propto \frac{NI\omega\left(\frac{Z_{\perp}}{Q}\right)Q}{B} \propto \frac{N(\text{gap width})}{(\text{pipe radius})^2},$$

where N is the number of accelerating cavities through which the beam passes, I is the beam current, ω is the frequency of cavity transverse modes, B is the axial magnetic field, and Q and Z_{\perp}/Q are cavity parameters defining the coupling impedance. In terms of cavity dimensions the most important parameters are the accelerating gap width and the pipe radius. The engineering impacts of this beam transport limitation are that careful attention must be given to low Q cell designs capable of high voltage gradients (with as low N and high field stress as possible) and that the cell structures must be large. Beam transport with chromatic aberrations implies $x(\tau, z) \propto \bar{x} \sin\Delta$, where $\Delta \propto \left(\frac{\Delta\gamma}{\gamma}\right)(\tau) \int k_{\beta} dz$; the beam displacement from center $x(\tau, z)$ is related to the beam offset and magnetic field errors (\bar{x}) and is also dependent on the integrated energy variation and phase advance through the entire accelerator. Here, the engineering premium is put upon energy regulation (minimizing $\frac{\Delta\gamma}{\gamma}$), alignment (minimizing \bar{x}),

and again in achieving maximum voltage gradient. Finally, emittance growth is generally most severe in the space-charge-dominated low energy regime where excess space charge fields can heat the beam. If one integrates through this regime of space-charge-dominated transport, the initial (ϵ_0) and final (ϵ) values of emittance are given by $\epsilon^2 = \epsilon_0^2 + K \frac{IR_b^2}{\gamma^3}$, where I is the beam current, R_b the beam size, γ the beam energy, and K is a parameter characterizing the details of the transport strategy which includes the beam profile and the rate at which (z dependent) the beam attains the high energy emittance-dominated regime. Again, high voltage gradient is obviously a premium. Even within these physics issues compromises are needed to resolve conflicting constraints, e.g., for minimum BBU growth the solenoidal field should be large but this requirement maximizes the phase advance concerns of the chromatic aberrations transport.

The realities of high average power operation pose additional challenges in the area of stray power management (duty factor, switching, energy regulation, accommodation of transients, operational integrity, etc.). These issues are being addressed on the ETA-II accelerator and the High Average Power (HAP) Test Stands. ETA-II (for illustrations, see other companion papers, e.g., KA1) is the 3-kA, 10-MeV, 50-ns, 5-kHz, 0.5-s burst duration facility that serves as our integration for achieving high-average-power linac induction accelerator operation. The power flow for ETA-II is schematically shown in Fig. 1: regulated dc power transiently energizes the capacitor bank of the command resonant charging (CRC) circuit which is switched into the intermediate energy storage (IES) capacitor, where it undergoes further time compression (several microseconds charging time). A magnetic modulator capable of 10-GW instantaneous and 2.5-MW average power performs final time compression. The induction accelerator cells present a nonlinear load to this power chain; both the time changing beam current and the ferrite response contribute to the load's nonlinear features. We next look in detail at the progress made in obtaining high average power operation for the various subassemblies comprising this power chain.

LIA Injector

ETA-II's injector is described in detail elsewhere, here we cover some of the unique operational features. Figure 2 illustrates the midplane of the injector, where the cathode surface

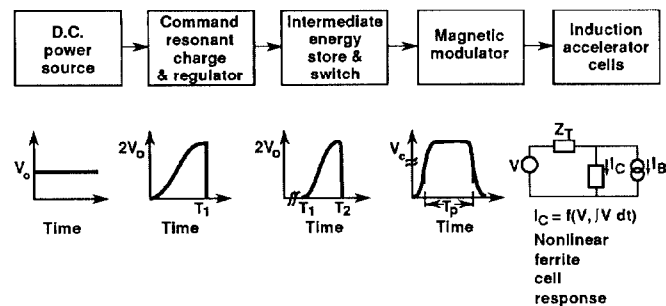


Fig. 1 Power flow for ETA-II.

*Work performed jointly under the auspices of the U.S. Department of Energy by Lawrence Livermore National Laboratory under contract W-7405-ENG-48 and for the Department of Defense Advanced Research Projects Agency ARPA Order No. 4395, monitored by Naval Surface Weapons Center.

[†] General Atomics

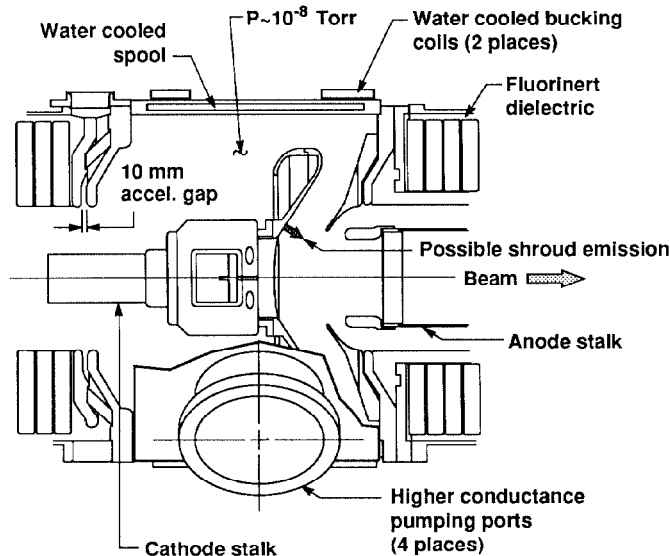


Fig. 2 Injector for ETA-II.

resides. The cathode is a $> 1100^\circ\text{C}$ osmium alloy dispenser and is held on a stalk that threads through five induction cells. The cathode faces an intermediate focusing electrode and then the anode bore, which is an extraction pipe that threads through four induction cells. With this arrangement a ~ 1 MeV acceleration potential occurs between the cathode and anode. Continued operation of the dispenser cathode at a space charge limited extraction current density of ~ 15 A/cm² requires good vacuum. Initial injector operation with freon as the cooling fluid showed that Freon permeated vacuum seals and led to cathode poisoning (Fig. 3) and gradual lowering of the beam current. Increasing the cathode temperature would offset this poisoning but would shorten cathode life. To avoid this, greater pumping capacity was added. The mid-plane spool was equipped with a water cooling jacket, and Fluorinert was used as the cooling fluid. These improvements avoid all cathode poisoning phenomena.

Beam emittance is determined by the injector's cathode and electrode design and can be easily spoiled by faulty operation. Ideally, for low emittance beams, a small area cathode is desired; this conclusion follows from conservation of angular momentum [$P_\perp \equiv m_0 v_\perp(\text{source}) \equiv \gamma m_0 v_\perp$, where $v_\perp(\text{source})$ is the cathode's intrinsic temperature] and the definition of normalized emittance [$\epsilon_N = \beta\gamma R'R = \beta\gamma \left(\frac{v_\perp}{c}\right) R \equiv \frac{\beta}{c} v_\perp(\text{source}) R = 2 \times 10^{-3} R(\text{cm}) \sqrt{T_{ev}(\text{source})}$]. Thus, one approach to obtaining low emittance beams of a required current would be to minimize cathode size but increase the field stress (high voltage and small anode-to-cathode gap, thereby increasing the space-charge-limited current density by $V^{3/2}/d^2$). However, this approach leads to excessive field stress on the electrode surfaces, which results in unwanted emission. Electron emission from the Pierce-correction cathode shroud devastates beam emittance since these electrons are born at a large angle with respect to the laminar flow. When these electrons are captured by and phase-mix with the beam, they greatly increase beam emittance. Figure 4 shows simulations of how a small fraction of electrons (0.8% of the total beam current) emitted from the inner radius of the shroud are captured by the beam as it transports between the cathode and anode; this interaction results in strong emittance growth. To avoid this phenomenon injector designs use larger area cathodes with minimum field stress and precisely shaped cathodes and electrodes designed

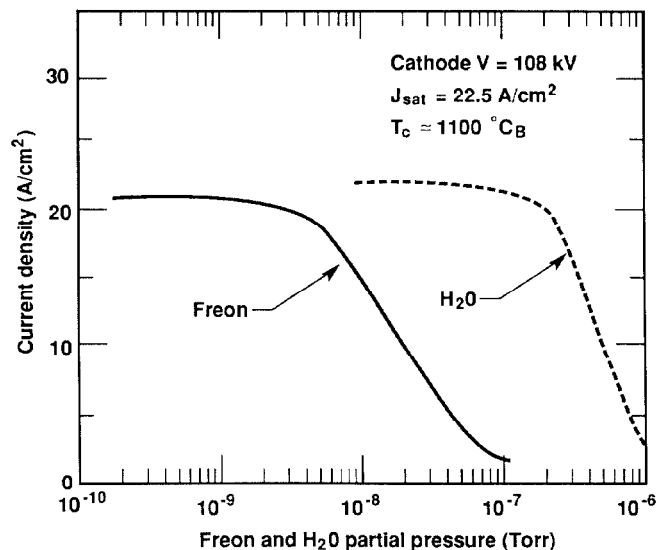


Fig. 3 Cathode poisoning (degradation of emission) in partial pressures of Freon and H₂O vapor.

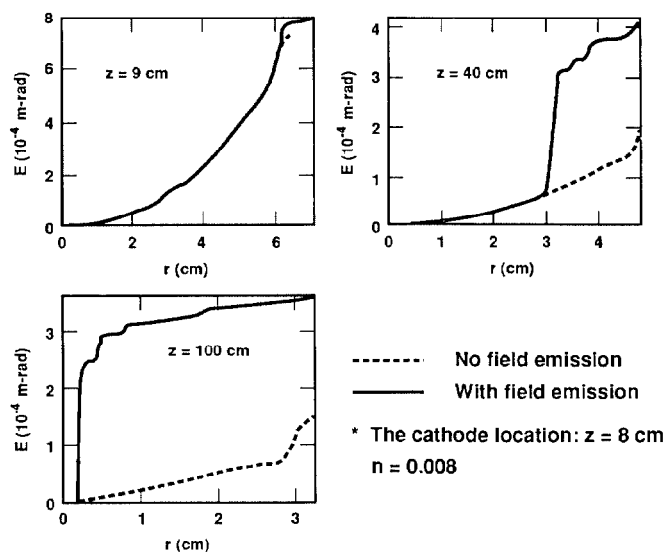


Fig. 4 Degradation of beam emittance with transport distance that results from mixing of a small fraction ($n = 0.8\%$) of electrons field-emitted from the shroud. Beam emittance is increased by approximately $1 + n$ (shroud emission angle/cathode temperature).

to avoid nonuniform beam profiles that enhance space-charge-driven emittance growth.

Referring again to Fig. 1, we see that part of the nonlinear accelerator core load is due to the electron beam itself. Thus, tailoring the beam current amplitude is a means of matching the nonlinear load and thereby achieving beam energy regulation. We are developing a method to modulate the beam current by modulating the accelerator voltage applied to the injector. The procedure is to preprogram the voltage in two of the injector's accelerator cores (one each on the cathode and anode side) and drive them with high voltage triode modulators. In so doing we can achieve a 5% beam current modulation, which will regulate the beam energy even though the load is nonlinear. Figure 5 shows experimental results from a prototype triode modulator; paralleling 16 such units yields

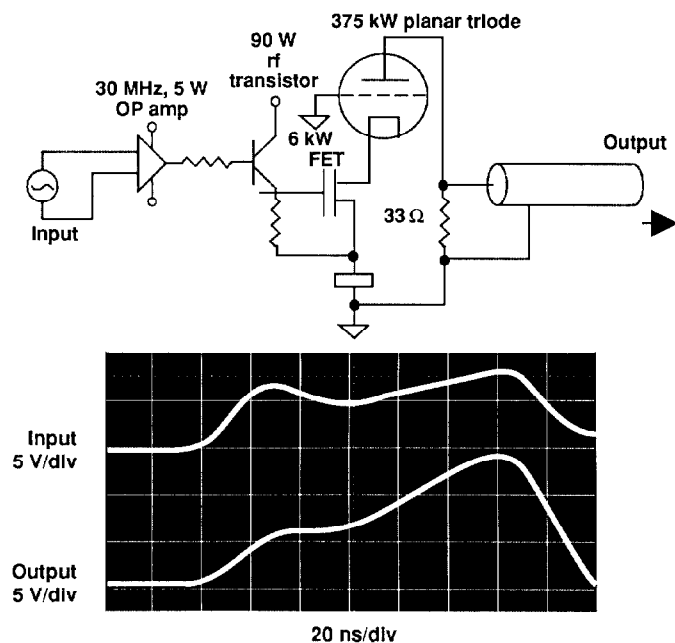


Fig. 5 Schematic and results of a prototype injector triode modulator.

sufficient power to drive the front and back accelerator cores of the ETA-II injector.

Accelerator Modules and Alignment

Figure 6 illustrates a single accelerator cell on ETA-II. These cells are assembled into 10-cell blocks connected by intercell pumping and diagnostic stations. Each focusing magnet must be aligned for minimum deviation (0.1 mm) of the central magnetic flux tube. This requires precision mechanical assembly of the individual cells comprising the 10-cell block, and then total alignment of all cell blocks. To accomplish this alignment we designate the mechanical center line with a helium-neon alignment laser and then plot the magnetic axis with a low energy electron beam. The difference between the laser and electron beam location is sensed by a movable television screen. In Fig. 7(a) we show the ~ 1.5 -mm deviation of an "uncorrected" magnetic flux tube. Referring to Fig. 5 we indicate that each individual solenoid is fitted with a sine/cosine pair of "correction" coils, which are separately energized to compensate field errors. Figure 7(b) shows the central flux tube derivation after using the correction coils; now the field alignment is ~ 0.1 mm. This same technique is used to align the entire accelerator assembly.

Also shown in Fig. 6 are the critical Al_2O_3 insulators and the narrow vacuum acceleration gap. We are experiencing lifetime degradation of these components. After months of operation some insulators acquire cracks, discharge tracks, and evidence of discharge plating, and some vacuum gaps show pittings and metallic blistering. Studies are under way to examine if field-enhancing triple-point junctions can be relieved and if lower dielectric constant insulators (or even resistive doped ceramics) can improved insulator lifetime integrity. We are evaluating whether the vacuum gap can be slightly increased in separation (but still consistent with tolerable BBU growth) and/or if different finishing procedures on the gap electrodes can decrease the susceptibility to arc formations that lead to surface degradation. These are ongoing studies, but the major activity is to develop electrical circuitry that absorbs all long

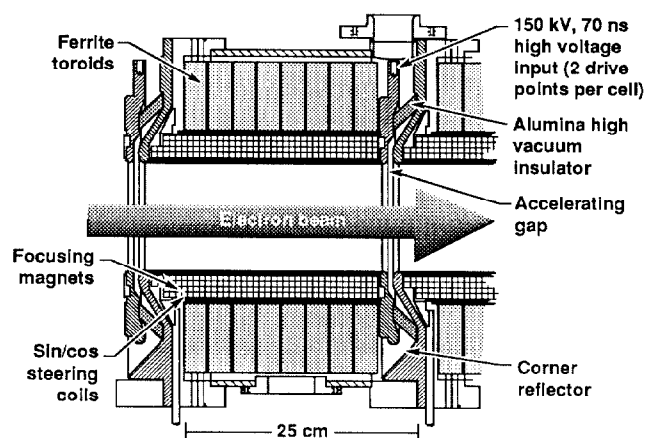


Fig. 6 ETA-II accelerator cell.

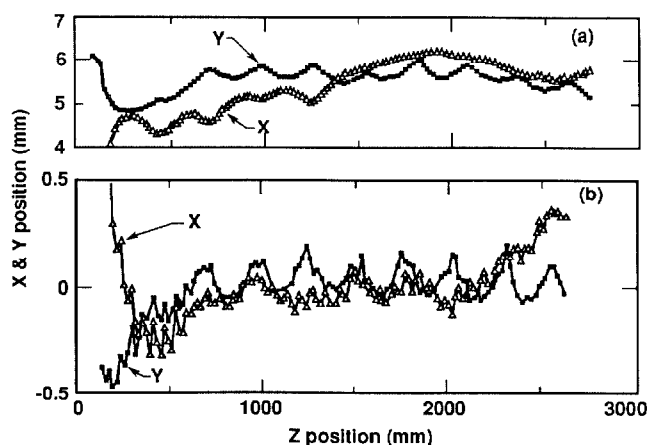


Fig. 7(a) and 7(b): Experimental measurements of the central magnetic flux tube for an ETA-II 10-cell block; (a) without correction coils, (b) with correction coils used - note the scale change.

lasting electrical power reflections and transients that could sustain arcs.

Pulse Power and Power Conditioning

In addition to modulating the beam current, our second approach to avoiding power reflections because of the nonlinear load of the accelerator cores is to taper the pulse forming line (PFL) within the magnetic modulators. Normally, the PFLs (which are actually water capacitors) are of constant geometry over the entire length that the discharging pulse travels, thereby giving constant impedance. By varying the geometry of the PFL we can vary the impedance of the discharging pulse to match the nonlinear ferrite response. Figure 8 shows results obtained when a sophisticated, nonlinear ferrite model was used to analyze a tapered PFL (impedance nonlinearly changing from 40 to 50 Ω) powering an accelerator core. The predicted accelerator voltage output is ± 2 kV out of ~ 286 kV. Such tapered PFL magnetic modulators will soon undergo tests in the HAP test stand facility.

Concerns for obtaining constant beam energy include issues that influence intrapulse and pulse-to-pulse energy variation. Because the volt-sec integral of the magnetic compressors is constant, both these energy variations are caused by timing errors whose sources include switch jitter, magnetic modulation input voltage variations, changes in the reset current, and

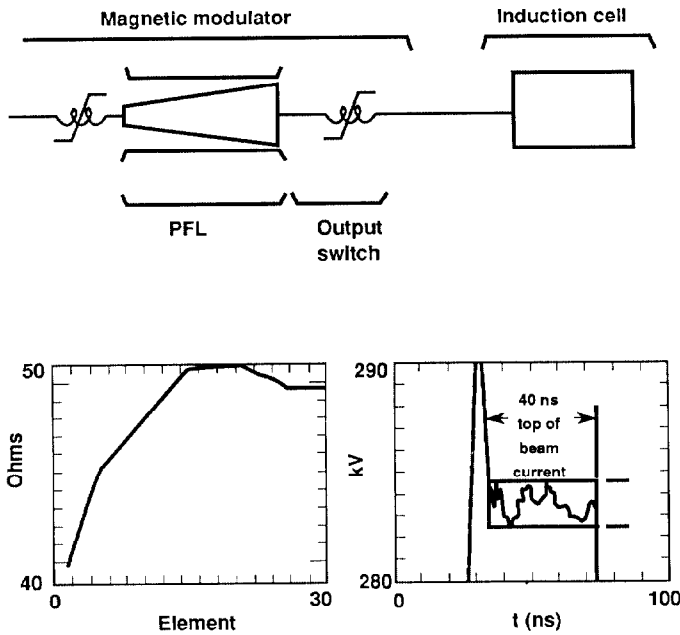


Fig. 8 Results of a circuit analysis of a tapered PFN for the magnetic modulator output stage.

drifts in switch or modulator delay due either temperature effects or to changes in magnetic materials. We show in Fig. 9 the circuit for ETA-II's thyatron modulators, which deliver power to the magnetic modulators; the four potential sources of timing errors are easily recognized in this schematic.

Thyatron switch jitter is of primary concern for the IES's CX 1547 tubes; for a single tube we measure the 1-sigma jitter as ~ 300 ps. To improve this we parallel several tubes. Test results confirm that two (three) parallel tubes have a 1-sigma jitter of ~ 190 ps (135 ps). Our present design uses two parallel tubes but has the capability of increasing this to four. All these tubes are thermal jacketed for uniform cooling.

Timing changes resulting from voltage variation of the CRC (the first stage modulator in Fig. 9) are corrected by a feed-forward technique illustrated in Fig. 10(a). In this circuit we linearize about the operating point the magnetic modulators' volt-sec characteristics and then determine an off-setting linear algorithm that is preprogrammed into a delay compensation comparative network. This network controls the gate to the IES's master trigger. Figure 10(b) illustrates the operational results of this circuit. With the IES capacitor voltage regulated to 1%, the magnetic modulator output voltage pulse has ~ 20 -ns jitter when no delay compensation network is used; when the compensator network is used, the observed jitter is ~ 1 ns.

A similar circuit (shown by dashes on Fig. 10(a)) is being designed for use as a feedback comparator to compensate for thermal drifts. Here, the sensor detects time shifts due to thermal effects on the magnetic modulator ΔB swings due to temperature rises. In this case the programmable delay advances the IES trigger so as to enable greater charging of the magnetic modulator input stage.

Referring again to the modulator circuit of Fig. 9, we see that the function of the CRC de-Q circuit is to clamp the IES charge voltage even if the dc input experiences ripple, drift, or loss of precision regulation. In spite of a 7% power supply regulation, the de-Q regulates the IES capacitor voltage to better than 0.04% under low repetition-rate operation (Fig. 11(a)).

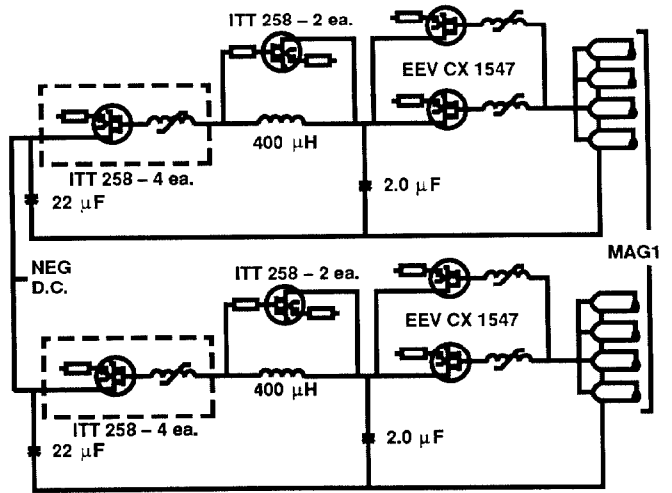


Fig. 9 ETA-II's thyatron modulator circuit.

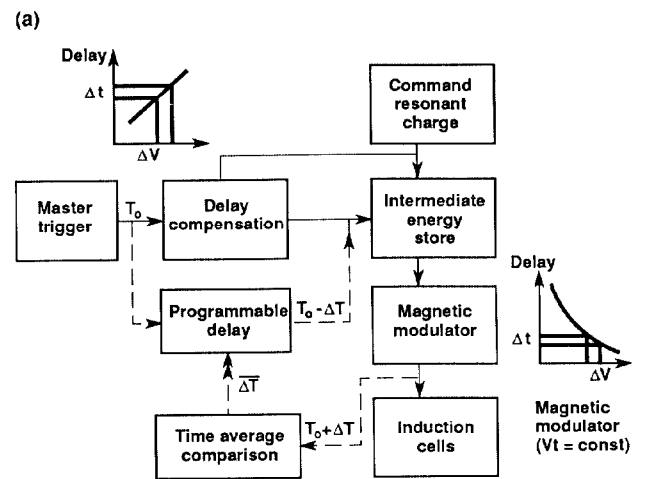


Fig. 10(a) Feed forward and feedback concepts to compensate for respectively changing voltage variations and thermal drifts.

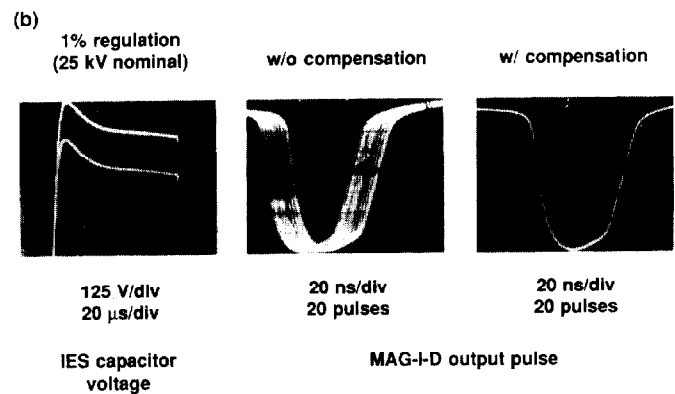


Fig. 10(b) Operational results of delay compensation circuit to reduce jitter.

However, at 5-kHz operation (Fig. 11(b)), the regulation degrades to $\sim 0.25\%$. This loss of de-Q ability at high repetition rate appears to result from noise-induced flutter on the reference signal or from a drift in the actual operating point. Both these possible causes are being evaluated on ETA-II as well as on the HAP test stand.

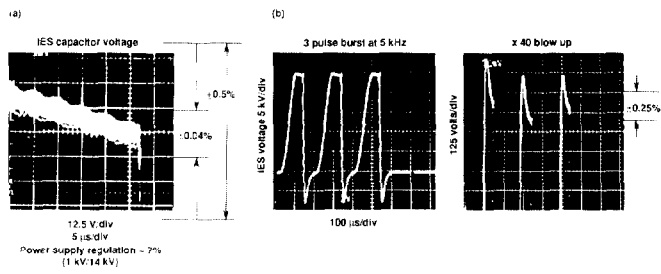


Fig. 11(a) Operational characteristics of de-Q circuit for low rep-rate; 11(b) Operational characteristics of de-Q circuit for 5 kHz rep-rate.

Consistent reset of all nonlinear magnetic elements, both in the magnetic modulators as well as the accelerator core itself, is also required for energy regulations so that precisely the same ΔB swing is used on every shot. Figure 12(a) shows the extreme ~ 80 -ns jitter in magnetic modulators (firing into a resistive dummy load) that occur when reset by a 5% regulated supply; this is contrasted to the 5-ns variation characterizing a 0.2% regulated reset supply. Actual measurements of the magnetic modulator timing error dependence on the reset current show the sensitivity of reset regulation — a 1-A change in reset current results in a 500-ps timing variation (Fig. 12(b)). For low-repetition rate-operation, highly regulated reset supplies are adequate; however, for high-repetition rate operations the existence of reflected power and/or persistent transients can offset this reset regulation.

Figure 13 shows an example of stray reflected power and how it is absorbed by a diode-clamp dissipative circuit that will assist reset. The voltage waveform indicates the switching characteristics of the input precompression stage of the magnetic modulator. Without a dissipative clamp, the reflected power will cause the core reset level to be repetition-rate dependent; with the clamp in operation the beam voltage is

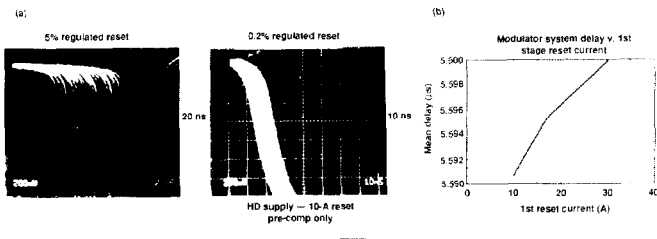
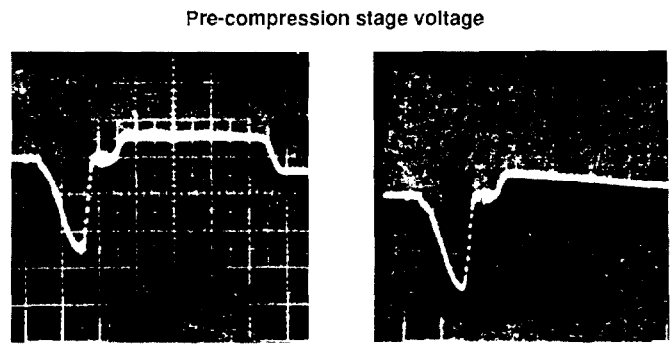
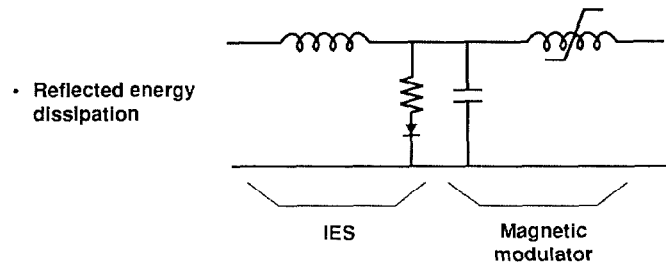


Fig. 12(a) Examples of magnetic modulator output jitter for two different regulators on the reset supplies; 12(b) Measured dependence of reset current versus output delay which illustrates the critical need for reset regulation.



10 kV, 5 μ s,
no clamp

10 kV, 5 μ s,
with clamp



• Reflected energy
dissipation

IES

Magnetic
modulator

Fig. 13 Example showing reflected power (which would alter reset conditions) and the benefit of the diode-clamp circuit being used on ETA-II.

maintained unipolar and rapidly decaying, thereby allowing for the reset condition to be sensed and, if need be, corrected. These types of circuits, which are necessary for reliable high repetition-rate operation, are being developed in the HAP test stand. HAP life tests have gradually been increasing in both run duration and repetition rate; to date the extrema of performance are bracketed by 0.6 sec operation at 500 Hz and ~ 10 ms operation at 5000 Hz.

Summary

Designs for LIAs stem primarily from physics concerns on stable beam transport and emittance preservation; these concerns yield specific design features of the induction cores and injectors, stringent requirements on energy regulation, and specification of voltage gradient and precision magnetic alignment. Further challenges unique to HAP operation (e.g., transient suppression, thermal management) heighten requirements on switching, reset regulation, jitter, power regulation/compensation, diagnostic sensing and active control. We have reviewed how our HAP test stands and the total system integration on ETA-II are developing the technologies needed to satisfy these requirements.